The 3D atlas builder: a dynamic and expandable 3D tool for monitoring the changes in the neuronal differentiation domain during hindbrain morphogenesis

Matthias Blanc[1], Frederic Udina[2,3] and Cristina Pujades[1*]

[1]Department of Experimental and Health Sciences, [2]Department of Economics and Business, Universitat Pompeu Fabra, Barcelona, Spain; [3]Data Science Center, Barcelona Graduate School of Economics, Barcelona, Spain

*corresponding author

*Correspondence to:

Cristina Pujades, PhD

Department of Experimental and Health Sciences

Universitat Pompeu Fabra

PRBB, Dr Aiguader 88, 08003 Barcelona, SPAIN

cristina.pujades@upf.edu

ORCID ID CP: 0000-0001-6423-7451

Running title: 3D-atlas builder: 3D monitoring of neuronal differentiation

Key words: morphogenesis, neuronal differentiation, neural progenitors, zebrafish, temporal 3D imaging

Summary statement

Brain morphogenesis studies can use our atlas-builder tool, which precisely maps cell populations in the embryonic brain over time and can be easily shared.

ABSTRACT

Reconstruction of prototypic three-dimensional (3D) atlases at the scale of whole tissues or organs requires specific methods to be developed. We have established a protocol and provide experimental proof for building a digital 3D atlas (here, for zebrafish hindbrain) that integrates spatial and temporal data for neuronal differentiation and brain morphogenesis, through a combination of *in vivo* imaging techniques paired with image analyses and segmentation tools. First, we generated a reference 3D hindbrain from several imaged specimens and segmented them using a trainable tool; these were aligned using rigid registration, revealing distribution of neuronal differentiation patterns along the axes. Second, we quantified the dynamic growth of the neuronal differentiation domain vs. the progenitor domain in the whole hindbrain. Third, we used *in vivo* Kaede-photoconversion experiments to generate a temporal heatmap of the neuronal growth in the whole hindbrain, revealing the spatiotemporal dynamics of neuronal differentiation upon morphogenesis. Last, as proof-of-concept, we assessed the birthdate order of GABAergic neurons using our temporal registration map. As this protocol uses open-access tools and algorithms, it can be shared for standardized, accessible, tissue-wide cell population atlas construction.

INTRODUCTION

Generating a precise cartography of cell populations in the embryonic brain is essential for understanding how brain morphogenesis impacts the position, and therefore function, of neuronal progenitors and neuronal clusters in normal and pathological conditions. Pioneer work in Drosophila provided 3D registration atlases and software that can automatically find the corresponding landmarks in a subject brain and map them to the coordinate system of a target brain (Peng:2011hc; Heckscher et al., 2014). In vertebrates, however, one of the main added challenges is to understand how time —and therefore tissue morphogenesis, as depicted by gene expression— impacts groups of cells. Critically, it must be taken into account that the generation of brain cell diversity occurs at the same time as the brain undergoes a dramatic transformation from a simple tubular structure (e.g., the neural tube) to a highly convoluted structure (e.g., the brain). Thus, one of the main unsolved questions is how gene expression and morphogenesis are coordinated (that is, the generation and maintenance of multiple cell types, in highly organized spatial patterns during brain embryonic development). Existing gene expression and marker atlases in fish provide valuable tools (Chow et al., 2020; Jaggard et al., 2020; Ronneberger et al., 2012; Tabor et al., 2019), but they typically have some limitations in addressing the question of spatiotemporal coordination, including: i) they are based on images from fixed samples acquired at late developmental stages and aligned through non-rigid registration, which is suboptimal for morphogenesis studies; ii) they use filters and are unable to quantify patterns, partially due to the lack of a standardized quantification method; iii) accessing the data is difficult; iv) user-upgrades are difficult, as data usually need to be sent to the atlas-makers for processing; v) atlases are usually hosted on individual platforms, making access to the data challenging; and vi) they lack 3D quantifications. Here, we developed a new “atlas-builder” pipeline that overcomes most of these limitations and can be used to create an expandable atlas of any tissue in any organism. Further, it can perform data analysis and quantification on a single platform, FIJI, which is already established as the standard for image analysis in the field. By keeping our pipeline in the FIJI eco-system, we aim to help share data, upgrade methodology and adapt the pipeline to a specific experimental set up (model organism, organ etc), thereby making it accessible to anyone.

Specifically, we generated an expandable 3D hindbrain atlas, taking advantage of the experimental toolkit available for zebrafish and combining *in vivo* images from transgenic embryos expressing a fluorescent reporter in differentiated neurons, with the Trainable Weka Segmentation 3D (TWS) (Arganda-Carreras et al., 2017), and the Fijiyama registration tool (Fernandez and Moisy, 2020). TWS is a machine learning tool that leverages a limited number of manual annotations and permits data to be automatically segmented after a short training, in order to quantify tissue volumes; the Fijiyama registration is an alignment tool that allows multi-modal rigid registration.

Our aim was to monitor the dynamic neuronal differentiation growth in the context of the brain, and to further pursue how cell differentiation and morphogenesis might be intertwined. Here, we made use of the zebrafish embryonic brainstem—the hindbrain, which undergoes a segmentation process along the anteroposterior (AP) axis leading to the formation of seven metamers called rhombomeres (Fraser et al., 1990; Jimenez-Guri and Pujades, 2011; Jimenez-Guri et al., 2010; Kiecker and Lumsden, 2005; Pujades, 2020). The first neuronal differentiation events in the hindbrain are observed just prior to 24 hours post-fertilization (hpf), with a pronounced increase of events from 30 hpf onwards, concomitant with dramatic morphogenetic changes (Belzunce et al., 2020). Neuronal differentiation in the hindbrain needs to be finely tuned, as it involves changes in proliferative capacity, an extraordinary displacement of neurons from their birth site and complex tissue morphogenetic movements over time. Although previous work has evoked the importance of neuronal birthdate in ascribing neuronal position within specific hindbrain circuits (Kinkhabwala et al., 2011; Pujala and Koyama, 2019), little is known about the role that time plays in the organizing differentiated neurons within this structure.

Here, we registered experimental whole hindbrain images and mapped neuronal differentiation patterns with a unified spatial representation. Specifically, we used a confocal microscopy imaging setup and cross-platform segmentation and registration tools. This dynamic neuronal differentiation map revealed the remodeling of the neuronal progenitor and neuronal cluster domains over time. By generating heatmaps of neuronal differentiation growth, we unveiled the temporal gradient of neuronal differentiation and provided an expandable 3D hindbrain atlas. Finally, as a proof-of-concept, we demonstrated that we could infer the birthdate of a given neuronal population by using this reference 3D atlas and a transgenic fish in which the GABAergic neurons are labeled. We believe that this

platform -the 3D atlas builder- will allow the integration of the information generated in other laboratories gained at different developmental stages. This collaborative integration is essential for expanding our overall knowledge about how the brain is functionally organized, and therefore advancing brain research, medicine and brain-inspired information technology.

RESULTS AND DISCUSSION

Building upon previous work that reconstructed prototype 3D atlases of whole embryos in Drosophila (Peng:2011hc; Heckscher et al., 2014), we aimed to generate a precise cartography of cell populations in the embryonic brain in zebrafish, to analyse in detail brain morphogenesis. Specifically, we combined genetic and *in vivo* imaging techniques with image-analysis tools to construct a 3D zebrafish hindbrain atlas, which revealed the remodeling of the neuronal progenitor and neuronal cluster domains upon time.

Developing a standardized, reliable 3D-image processing and quantification method

We planned to acquire large image dataset with state-of-the-art light microscopy. First, quantitatively evaluating these datasets often involves manually annotation, which is time-consuming, introduces biases and often constitutes the major bottleneck in an evaluation pipeline. To overcome this problem, we used the Trainable Weka Segmentation 3D (TWS, (Arganda-Carreras et al., 2017), which combines the image processing toolkit FIJI (Schindelin et al., 2012) with the state-of-the-art machine learning algorithms provided in the latest version of the data mining and machine learning toolkit Waikato Environment for Knowledge Analysis (WEKA) (Hall et al., 2009). The advantage of this tool is that it is modular, allows sophisticated data mining processes to be built up from the wide collection of base learning algorithms and tools provided, is open-sourced and can be easily used as a plugin of FIJI. Second, the comparison of various signals across specimens requires an alignment/registration, which is often done manually and is very time-consuming. To overcome this problem, we used the Fijiyama plugin in FIJI, which allowed multi-modal automatic rigid registration process and a large range of customization (Fig. 1).

Our aim was to develop a working pipeline that allowed us to segment and isolate specific signal from *z*-stack images in a semi-automatic manner in order to: i) quantify the specific signal in different specimens, ii) generate a reference zebrafish hindbrain 3D model, iii) use this reference 3D model for further registrations and comparisons, and iv) combine reference 3D models to generate a 3D atlas. For this, we used images from zebrafish *Tg[HuC:Kaede]* embryo hindbrains, which displayed Kaede in the whole neuronal differentiation domain. 3D images were then acquired from different specimens (s1–sY; *n*=5), and different users (u1–uX; *n*=4) were invited to use the TWS tool to train classifiers

(one per user) in order discern noise vs. signal in the raw data obtained for each specimen (Fig. 1). Accordingly, as many binary 3D masks of the same image as users were generated (*n*=4). These binary 3D masks (from different users) were then averaged to assess the specimen 3D model (with this process repeated as many times as the specimen number). Specimen 3D models were registered, the volume of the specific signal was quantified and specimen 3D models were averaged (in our case, averaging 4 specimens) to finally obtain the label "3D model", which contains the merged information from all specimens (s1–sY). Thus, we generated as many reference 3D models as specimens to be compared, by reiteration of the whole process. Finally, we compared spatiotemporal distribution of the labeling signals between specimens and built up the reference 3D-atlas. This automatic segmentation and registration allowed us to: i) assess signal similarity between segmentations to limit the bias due to the individual subjectivity, ii) obtain reliable quantification at the tissue level, iii) produce a representative model of a label and estimate inter-individual variability, and finally iv) build up a reference brain to be further used for spatiotemporal comparisons.

The neuronal differentiation domain dramatically increases at the expense of the progenitor domain

Next, we wanted to apply our pipeline to monitor the dynamic growth of the neuronal differentiation domain (NDD). First, we did a spatiotemporal analysis of the growth of the NDD domain by Kaede photoconversion experiments. We made use of *Tg[CAAX:GFP;HuC:Kaede]* embryos, in which Kaede^{Green} was fully photoconverted to Kaede^{Red} at different embryonic stages, to assess time-interval encompassing neurogenesis, neuronal differentiation and morphogenetic changes (24 to 72 hpf; Fig. 2); here, differentiated neurons were labelled in magenta, and the whole hindbrain, in green. After Kaede photoconversion, five embryos for each stage were imaged at 24, 36, 48 and 72 hpf, and the datasets underwent the previously described pipeline (e.g., images from embryonic hindbrains at each different stage were registered, and the size of both the progenitor, PD and the NDD were assessed by quantifying the generated reference 3D models). The NDD was segmented as described in our pipeline in Fig. 1; however, due to the sparse CAAX:GFP labeling (which is membrane labelling, rather than cytoplasm labelling as for the other signals), the overall hindbrain was manually segmented using a homemade macro, which

implied interpolating a dozen of manually segmented sections across the stack (see macro, Supplementary Material; note that even such a difficult signal could be segmented with TWS 3D at the expense of computing power). As shown in Fig. 2, the NDD dramatically increased during this time period, consistent with previous qualitative descriptions (Belzunce et al., 2020; Lyons et al., 2003; Voltes et al., 2019). Only few cells underwent differentiation before 24 hpf (Fig. 2A, V_{NDD} = 1.67 ($\pm$ 0.26) $\times 10^6$ μm^3 vs. V_{PD} = 4.72 ($\pm$ 0.21) $\times 10^6$ μm^3 at 24 hpf; Fig. 2B-B', see green-PD and magenta-NDD as representative examples of raw data of a single embryo at two different positions, r3 and r5, along the AP axis). However, this situation dramatically changed few hours later: at 36 hpf, we observed that the size of the NDD was higher than the PD (Fig. 2A, V_{NDD} = 6.77 ($\pm$ 1.08) $\times 10^6$ μm^3 vs. V_{PD} = 3.45 ($\pm$ 0.43) $\times 10^6$ μm^3 at 36 hpf; Fig. 2C-C', compare green and magenta domains). By 48 hpf and 72 hpf, the differentiated neurons mostly occupied the whole hindbrain (Fig. 2D-D', E-E'). This dramatic increase of the NDD (Fig. 2A, V_{NDD} = 10.36 ($\pm$ 0.72) x 10^6 μm^3 at 48 hpf and V_{NDD} = 14.48 ($\pm$ 0.69) $\times 10^6$ μm^3 at 72 hpf), was at expense of the PD. Further, this depletion of the PD between 24hpf and 48hpf could be clearly appreciated in the quantified volumes (Fig. 2A; V_{PD} = 1.96 [$\pm$ 0.52] $\times 10^6$ μm^3 at 48 hpf), and this decrease was sustained until 72 hpf (V_{PD} = 0.99 ($\pm$ 0.32) $\times 10^6$ μm^3 at 72 hpf). Thus, differentiated neurons populated the whole hindbrain in an approximately 48-h span of time (from 24 to 72 hpf); while the PD occupied a huge part of the hindbrain at 24 hpf, it was almost entirely depleted by 72 hpf. This remodeling could be better observed by plotting the ratios of the PD and the NDD over the entire hindbrain (Fig. 2F, G).

Neuronal birthdate dictates the spatial distribution of differentiated neurons within the hindbrain

Previous work has shown the importance of neuronal birthdate in ascribing neuronal function: i) the stripe patterning of *alx*-expressing neurons, which are involved in swimming behavior, is age-related (Kinkhabwala et al., 2011), and ii) the V2a cell body position and order of spinal projections in the hindbrain relies on their neuronal birth (Pujala and Koyama, 2019). Thus, we wanted to explore whether the temporal order of differentiation prefigured the further spatial allocation of differentiated neurons. We performed spatiotemporal analyses of neuron birthdating using Kaede photoconversion experiments as

a tool to register temporality. In this case, the Kaede protein in *Tg[HuC:Kaede]* embryos was completely photoconverted at different developmental stages (24, 36 or 48hpf), and embryos were analyzed either at 48 hpf or at 72 hpf (at which point the majority of the progenitor cells were extinguished) (Fig. 3). This allowed us to assess the relative position of Kaede^{Red}-cells (early-born neurons; in magenta) vs. Kaede^{Green}-cells (late-born neurons; in green), and provided us with another layer of complexity (in comparison with Fig. 2), since it informed us how neurons born at different stages organized at 72hpf. When we analyzed embryos at 48 hpf, we observed that early-born neurons were located more ventrally and medially than late-born cells (Fig. 3A, C; see magenta cells). Moreover, a specific dorsoventral (DV) column could be observed in rhombomeres 4 to 6, with neurons born between 24 and 36 hpf reaching the ventricular zone (Fig. 3C, see white asterisk). To further analyze the remodeling of the neuronal differentiation territory, we generated the reference 3D models of the early-born (24 hpf) and late-born (36 hpf) territories in the context of the whole differentiated neuronal domain (Fig. 3B-B', D-D'), and obtained information about its dynamics (Fig. 3E). We could observe the inner–outer gradient of neuronal differentiation, in which younger neurons were deposited dorsally and laterally of older neurons (Fig. 3B-B', D-D'; see late-born neurons in white vs. early-born neurons in black). Moreover, 3D models supported the overall consistency of patterns across samples, strongly suggesting that neuronal birthdate restricted the spatial distribution of differentiated neurons. When we assessed the volume sizes (Table 1), we detected that, of the whole differentiated domain at 48 hpf (approximately $V_{NDD} = 12.25 \times 10^6\ \mu m^3$), only a small territory comprised neurons differentiated before 24 hpf ($2.67\ [\pm\ 1.05] \times 10^6\ \mu m^3$ early-born neurons vs. $9.58\ (\pm\ 1.24) \times 10^6\ \mu m^3$ late-born neurons), whereas most of the differentiated neurons arose before 36 hpf ($9.53\ [\pm\ 0.72] \times 10^6\ \mu m^3$) and the rest differentiated between 36 and 48 hpf ($3.86\ [\pm\ 0.53] \times 10^6\ \mu m^3$). This growth in the differentiated neuronal domain could be clearly observed when the relative contribution of early- vs- late-born neurons as compared to the whole neuronal differentiation territory at 48 hpf was assessed (Fig. 3E).

To seek how different birthdated neurons changed position during morphogenesis, we expanded our study to the timepoint at in which most of the cells have already differentiated (e.g., 72 hpf). As before, we observed that early differentiated neurons were

located more ventrally and medially, and that late-born cells piled up (Fig. 3F, H, J; see magenta cells). The same specific DV column of early differentiated neurons was observed in the rhombomeres 4 to 6 (Fig. 3H, J; see white asterisk). Next, to determine whether the temporal order of neuronal differentiation prefigured the spatial distribution of neurons in the tissue, we compared the label 3D models of the neuronal domains generated at 24 hpf, 36 hpf and 48 hpf in the context of the whole differentiated neuronal domain at 72 hpf, by overlapping and color-coding them according to the neuronal birthdate (Fig. 3G-G', I-I', K-K'; see young neurons in white vs. old neurons in black). The overlaying maps showed that i) most of the neuronal differentiation events occurred between 24 and 48 hpf, and ii) early-born neurons were always located in the inner part of the differentiation domain and were surrounded by younger neurons, generating an inner–outer gradient of early-born vs. late-born neurons. This suggested that the position of neurons relied on their neuronal birthdate, and demonstrated the importance of morphogenesis for remodeling the differentiation domain. When volumes were quantified at 72 hpf (Table 2), we observed that only a small part of the NDD came from neurons born before 24 hpf (3.63 ($\pm$ 1.30) $\times 10^6$ μm^3 for early-born neurons vs. 12.81 [$\pm$ 2.15] $\times 10^6$ μm^3 for late-born neurons). Most neurons underwent differentiation between 24 hpf and 48 hpf, with half of the differentiated neurons arising before 36 hpf (7.8 ($\pm$ 1.7) $\times 10^6$ μm^3 neurons born before 36 hpf vs. 7.08 ($\pm$ 1.43) $\times 10^6$ μm^3 after 36 hpf) and the rest were differentiated between 36 and 48 hpf (11.65 ($\pm$ 1.42) $\times 10^6$ μm^3 neurons born before 48 hpf vs. 3.19 [$\pm$ 0.43] $\times 10^6$ μm^3 after 48 hpf). This continuous birth of differentiated neurons could be clearly observed by assessing the relative contribution of early- vs. late-born neurons as compared to the whole NDD (Fig. 3L). Overall, these results indicated a consistency of birthdate patterns across samples, suggesting that the positions of differentiated neurons in the inner–outer differentiation gradient was linked to their birthdate.

To monitor possible differences in the spatial distribution within the neuronal differentiation along the different body axes (antero-posterior, AP; medio-lateral, ML; and dorso-ventral, DV) we took sample segmentations from the previous birthdate experiments (Fig. 3F, H, J), and created virtual "slices" along the different axes for sampling signal position (Fig. 3M; the number of virtual slices along the given axis is indicated on the X-axis). We observed that the domains corresponding to early- vs late-born neurons followed the

same trend (e.g., the red, green and blue lines did not display major changes in the multiple virtual slices), with no main differences along the AP or ML axes (Fig. 3M). As expected, when the analysis was performed along the DV axis of the differentiation domain, differences in allocation relying on the neuronal birthdate could be appreciated, with early-born neurons (24 hpf) displaying a ventral enrichment (Fig. 3M, see DV-axis graph). Overall, these whole population analyses allowed us to better understand the intertwinement of morphogenesis and cell behaviors.

The 3D atlas of temporal differentiation can be used as a proxy to infer neuronal birthdates

Our next goal was to investigate whether position in the neuronal differentiation domain could be used as a proxy for neuronal birthdating. For this, we first built up a temporal 3D atlas of neuronal differentiation using the 3D models previously generated (Fig. 4) at 48 hpf and 72 hpf. First, we generated the 48 hpf 3D atlas by overlaying the neuronal differentiation 3D models generated from neurons born at 24 hpf and 36 hpf, and color-coded according to the birthdate (Fig. 4A-A''; black: neurons born before 24 hpf, magenta: neurons born 24-36 hpf, and white: neurons born between 35 and 48 hpf). As expected, the late-born neurons were peripherical allocated (see white cells in Fig. 4A-A''). Second, we built up the 72 hpf 3D atlas using the same strategy: overlaying the 3D models displaying cells differentiated at 24, 36, or 48 hpf (Fig. 4B-B'', C-C'', D-D''). We clearly observed that there was cell differentiation between 24 and 36 hpf all along the AP axis (Fig. 4B-B''; see white domain) and that this differentiation capacity diminished with time (Fig. 4C-C''; see small white domain); indeed, by 48 hpf, almost the whole differentiation domain was already occupied by previously-born neurons (Fig. 4D-D''; see black territory). We could also observe that an important part of neurons born between 48 and 72 hpf were located in rhombomere 1 (Fig. 4C''-D''), which was confirmed by the AP distribution (Fig. 3M; see the high ratio of 48hpf line at the most anterior domain).

Thus, this temporal registration provided important advantages, as it allowed us to: i) dissect the final location of birthdated populations with high precision, ii) obtain a whole-population coverage, and iii) maintain *in vivo* structure positioning. Until now, most of the currently used approaches lack whole-cell population coverage, have poor temporal precision and are limited by expression timing of the gene or transgene; more importantly,

although they permit coverage of the whole cell population, they do not allow the user to foreshadow the birthdate of a given population at the time of interest. In the future, our method can be further improved by using batch processing algorithm (e.g., to assess the effects of pharmacological treatments or gene disruptions) or by adjusting for more geometrically complex tissues or for tissues with less alignment features (such as heart). Last but not least, this pipeline can be applied to time-lapse videos by repeating the process for each frame.

As a proof-of-concept, we used the *Tg[gad1b:DsRed]* line that displays DsRed in the GABAergic neurons (Satou et al., 2013). To dissect when GABAergic neurons were born, we generated an label 3D model of *Tg[gad1b:DsRed]* embryos at 72 hpf, and overlayed it on the temporal 3D maps generated in Fig. 4. As observed in Fig. 5, gad1b was mainly located in the neuronal differentiation territory with neurons born between 24 and 36 hpf (Fig. 5A-A', B-B', see white-colored region), with some in r5 being born as early as 24 hpf (Fig. 5A'). Analyzing the expression pattern of GABAergic neurons according to DsRed expression in *Tg[gad1b:DsRed]* embryos, we observed that there were many GABAergic cells at 72 hpf (Fig. 5D) but not very many at 48hpf (data not shown), suggesting that (as expected) the expression of DsRed in the *Tg[gad1b:DsRed]* line was delayed (note that this is common in transgenic lines). To demonstrate that this was the case, we performed *in situ* hybridization with *gad1b* at early stages and observed that, indeed, some GABAergic neurons were already specified in r3 and r5 at 24 hpf (Fig. 5E), demonstrating that this temporal differentiation 3D map could be used as a proxy to infer neuronal birthdate.

Usually, expression of the reporter genes in transgenic lines is delayed as compared to the gene expression onset, unless the reporter has been inserted within the given gene locus. Now, we can specifically knock-in genes within a targeted genome site thanks to the CRISPR-Cas9 technology, but most of the available—and very valuable—transgenic lines were (and are still) generated with insertion systems that do not recapitulate the temporal onset of gene expression. Thus, our tool can be very useful for predicting neuronal birthdates just by analyzing the position of neurons in the differentiation domain.

In summary, our 3D tool provides an established protocol using open-access tools and algorithms and allows construction of standardized, accessible, tissue-wide cell population atlases.

MATERIALS AND METHODS

Zebrafish strains

Zebrafish (*Dario rerio*) were treated according to the Spanish/European regulations for the handling of animals in research. All protocols were approved by the Institutional Animal Care and Use Ethic Committee (Comitè Etica en Experimentació Animal, PRBB) and the Generalitat of Catalonia (Departament de Territori i Sostenibilitat), and they were implemented according to European regulations. Experiments were carried out in accordance with the principles of the 3Rs.

Embryos were obtained by mating of adult fish using standard methods. All zebrafish strains were maintained individually as inbred lines. The *Tg[βactin:HRAS-EGFP]* line, denoted herein as *Tg[CAAX:GFP]*, has GFP in the plasma membrane and was used to label the cell contours (Dale and Topczewski, 2011). The *Tg[HuC:GFP]* (Park et al., 2000) and *Tg[HuC:Kaede]* (Harrison et al., 2014) lines were used to label differentiated neurons. The *Tg[gad1b:lox-DsRed-lox-EGFP]* line (denoted *Tg[gadb1:DsRed]* herein) was used to label GABAergic neurons with DsRed (Satou et al., 2013).

Photoconversion experiments

Prior to photoconversion, differentiated neurons were visualized by excitation for Kaede ^{Green} marked cells using a 488 nm laser. Photoconversion of the Kaede flourescent protein (from green to red) was performed using a Leica SP8 inverted confocal microscope by manually scanning one focal plane centered on the hindbrain with an 8 to 16 frame averages per image, under continuous laser scanning using a 405 nm laser. Proper photoconversion was monitored by the appearance of strong Kaede^{Red} signal under excitation with a 543 nm laser. As an internal control, the disappearance of Kaede^{Green} upon appearance of Kaede^{Red} was verified.

Whole-mount *in situ* hybridization and immunostainings

The *gad1b* riboprobe encompassing the nucleotides 1104-2334 of accession noAB183390 as described in (Zhang et al., 2020) was used. The *gad1b* template was generated by PCR amplification by adding the T7 promoter sequence (indicated by capital letter) to the reverse primer (*gad1b* Fw 5'-gat ggt tgc gcg gta taa-3'; *gad1b* Rev 5'-ata tta ata cga ctc act

ata gCT TCG TTA AAA GGG TGC-3'). For fluorescent *in situ* hybridization, the DIG-labeled probe was detected with TSA-Cy3. Cell nuclei were stained with DAPI.

Confocal imaging of life samples

Zebrafish embryos were treated with PTU at 24 hpf prior to being anesthetized with tricaine and mounted dorsally in 0.9% low melting point agarose at the desired time. Images were acquired with a Leica SP8 system using PMT detectors and a 20× glycerol immersion objective. HCX PL APO Lambda blue 20×/0.7 argon laser 30%, Diode 405nm (DPSS 561; Ready Lasers).

Stained fixed samples were mounted in 0.9% low melting point agarose on glass-bottom Petri dishes (Mattek) and imaged on a Leica SP8 inverted confocal microscope with 20× glycerol immersion objective and hybrid detectors. For x*yz* confocal cross-sections, *z*-stacks were acquired with a 1.194 µm *z* distance.

Image processing and analyses

Segmentation algorithm

The Trainable Weka Segmentation FIJI plugin (Arganda-Carreras et al., 2017), a machine learning tool for microscopy pixel classification, was used for image segmentation (Fig. 1). Training features for the algorithm were kept to mean and variance in order to limit compute power usage, insuring accessibility. Other training features can be considered for challenging signals and segmentation of structures within a single signal. First, classifiers from the very same specimen were generated from supervised training of the algorithm by different users. Random *Tg[HuC:Kaede]* embryo specimens at 72 hpf were used, in which Kaede was photoconverted at 24 hpf. Separate classifiers were trained for individual channels. The classifiers generated by the four users were then used to segment each sample and to obtain the average 3D-model from a single specimen. This process was repeated for each specimen (n = 5 specimens per sample). Training took about 4 min per step with around 3-4 steps to complete it, and generation of a mask through a single classifier took about 10 min on a consumer-grade workstation with an 3700X (8 cores, 16 threads, 3.6Ghz) AMD processor and RAM 32GB. Averaging across user's segmentations was

then performed, and signal with at least 50% homology across segmentations were quantified. The reference 3D maps could then be used for sample comparisons.

Registration algorithm

Fijiyama registration FIJI plugin (Fernandez and Moisy, 2020), a registration tool for 3D multimodal time-lapse imaging, was used with 4 steps of automatic rigid registration for each alignment: 2 steps without and 2 steps with subpixellic accuracy, oversized images subsampling was left on.

Tissue volume quantification

Specimen's 3D-models were registered together and resliced along different axes. Slices were then quantified using FIJI's 3D object counter. The slicing and quantification of individual slices was automatized with a simple homemade FIJI macro (see Supplementary Material and https://www.upf.edu/web/pujadeslab).

Statistical analysis

Statistical tests and graphical representations were done using the GraphPad Prism7 software. We used ratios of early-produced neuronal differentiated domain vs. total differentiation domain to fit a nonparametric regression curve with local linear kernel estimation method (Fan, 2018). The R (R core team 2020) package npregfast (Sestelo et al.) version 1.5.1, and the kernel Epanechnikov (with bandwidth parameter selected by cross-validation) were used.

ACKNOWLEDGEMENTS

The authors thank the current members of the Pujades lab for help in the training of the algorithms for Trainable Weka Segmentation and for critical insights. We wish to thank Dr. S Higashijima (National Institute for Basic Biology, Japan) and Dr. G Sumbre (IBENS) for kindly providing the transgenic line *Tg[gadb1:DsRed].*

CONFLICT OF INTERESTS

The authors declare no competing or financial interests.

FUNDING SOURCES

This work was funded by the Agencia Española de Investigación AEI-PGC2018-095663-B-I00 and RED2018-102553-T grants (MICIU-FEDER) to CP, and PGC2018-101643-B-I00 to FU. DCEXS-UPF is a Unidad de Excelencia María de Maeztu funded by the Agencia Española de Investigación (CEX2018-000792-M). MB is recipient of a fellowship from "Unidad de Excelencia María de Maeztu", funded by the Spanish Ministry of Science and Innovation (ref. MDM-2014-0370 and CEX2018-000792-M). CP is a recipient of ICREA Academia award (Generalitat de Catalunya).

DATA AVAILABILITY

All datasets supporting our work are included as Supplementary Figures and/or are available in our web site https://www.upf.edu/web/pujadeslab

AUTHOR CONTRIBUTIONS

MB and CP contributed to the conceptualization and design of experiments and analysis of results. MB carried out all the experiments and established the pipeline. FU contributed to the analysis of results. CP wrote the manuscript.

REFERENCES

Arganda-Carreras, I., Kaynig, V., Rueden, C., Eliceiri, K. W., Schindelin, J., Cardona, A. and Sebastian Seung, H. (2017). Trainable Weka Segmentation: a machine learning tool for microscopy pixel classification. *Bioinformatics* **33**, 2424–2426.

Belzunce, I., Belmonte-Mateos, C. and Pujades, C. (2020). The interplay of atoh1 genes in the lower rhombic lip during hindbrain morphogenesis. *PLoS ONE* **15**, e0228225.

Chow, D. M., Sinefeld, D., Kolkman, K. E., Ouzounov, D. G., Akbari, N., Tatarsky, R., Bass, A., Xu, C. and Fetcho, J. R. (2020). Deep three-photon imaging of the brain in intact adult zebrafish. *Nat Meth* **17**, 605–608.

Dale, R. M. and Topczewski, J. (2011). Identification of an evolutionarily conserved regulatory element of the zebrafish col2a1a gene. *Developmental Biology* **357**, 518–531.

Fan, J. (2018). *Local Polynomial Modelling and Its Applications*. Routledge.

Fernandez, R. and Moisy, C. (2020). Fijiyama: a registration tool for 3D multimodal time-lapse imaging. *Bioinformatics* **61**, 139.

Fraser, S., Keynes, R. and Lumsden, A. (1990). Segmentation in the chick embryo hindbrain is defined by cell lineage restrictions. *Nature* **344**, 431–435.

Hall, M., Frank, E., Holmes, G., Pfharinger, B., Reutemann, P. and Witten, I. H. (2009). The WEKA Data Mining Software: An Update. *SIGKDD Explorations* **11**, 10–18.

Harrison, C., Wabbersen, T. and Shepherd, I. T. (2014). In vivo visualization of the development of the enteric nervous system using a Tg(-8.3bphox2b:Kaede) transgenic zebrafish. *Genesis* **52**, 985–990.

Heckscher, E. S., Heckscher, E. S., Long, F., Long, F., Layden, M. J., Layden, M. J., Chuang, C. H., Chuang, C.-H., Manning, L., Manning, L., et al. (2014). Atlas-builder software and the eNeuro atlas: resources for developmental biology and neuroscience. *Development* **141**, 2524–2532.

Jaggard, J. B., Lloyd, E., Yuiska, A., Patch, A., Fily, Y., Kowalko, J. E., Appelbaum, L., Duboue, E. R. and Keene, A. C. (2020). Cavefish brain atlases reveal functional and anatomical convergence across independently evolved populations. *Sci Adv* **6**, eaba3126.

Jimenez-Guri, E. and Pujades, C. (2011). An ancient mechanism of hindbrain patterning has been conserved in vertebrate evolution. *Evolution & Development* **13**, 38–46.

Jimenez-Guri, E., Udina, F., Colas, J.-F., Sharpe, J., Padrón-Barthe, L., Torres, M. and Pujades, C. (2010). Clonal analysis in mice underlines the importance of rhombomeric boundaries in cell movement restriction during hindbrain segmentation. *PLoS ONE* **5**, e10112.

Kiecker, C. and Lumsden, A. (2005). Compartments and their boundaries in vertebrate brain development. *Nature Reviews Neuroscience* **6**, 553–564.

Kinkhabwala, A., Riley, M., Koyama, M., Monen, J., Satou, C., Kimura, Y., Higashijima, S.-I. and Fetcho, J. (2011). A structural and functional ground plan for neurons in the hindbrain of zebrafish. *Proc. Natl. Acad. Sci. U.S.A.* **108**, 1164–1169.

Lyons, D. A., Guy, A. T. and Clarke, J. D. W. (2003). Monitoring neural progenitor fate through multiple rounds of division in an intact vertebrate brain. *Development* **130**, 3427–3436.

Park, H. C., Kim, C. H., Bae, Y. K., Yeo, S. Y., Kim, S. H., Hong, S. K., Shin, J., Yoo, K. W., Hibi, M., Hirano, T., et al. (2000). Analysis of upstream elements in the HuC promoter leads to the establishment of transgenic zebrafish with fluorescent neurons. *Developmental Biology* **227**, 279–293.

Pujades, C. (2020). The multiple functions of hindbrain boundary cells: Tinkering boundaries? *Seminars in Cell and Developmental Biology* **107**, 179–189.

Pujala, A. and Koyama, M. (2019). Chronology-based architecture of descending circuits that underlie the development of locomotor repertoire after birth. *Elife* **8**, 471.

Ronneberger, O., Liu, K., Rath, M., Rueβ, D., Mueller, T., Skibbe, H., Drayer, B., Schmidt, T., Filippi, A., Nitschke, R., et al. (2012). ViBE-Z: a framework for 3D virtual colocalization analysis in zebrafish larval brains. *Nat Meth* **9**, 735–742.

Satou, C., Kimura, Y., Hirata, H., Suster, M. L., Kawakami, K. and Higashijima, S.-I. (2013). Transgenic tools to characterize neuronal properties of discrete populations of zebrafish neurons. *Development* **140**, 3927–3931.

Schindelin, J., Arganda-Carreras, I., Frise, E., Kaynig, V., Longair, M., Pietzsch, T., Preibisch, S., Rueden, C., Saalfeld, S., Schmid, B., et al. (2012). Fiji: an open-source platform for biological-image analysis. *Nat Meth* **9**, 676–682.

Sestelo, M., Villanueva, N. M., Softw, L. M.-M. J. S.2017 npregfast: An R package for nonparametric estimation and inference in life sciences. *jstatsoft.org*

Tabor, K. M., Marquart, G. D., Hurt, C., Smith, T. S., Geoca, A. K., Bhandiwad, A. A., Subedi, A., Sinclair, J. L., Rose, H. M., Polys, N. F., et al. (2019). Brain-wide cellular resolution imaging of Cre transgenic zebrafish lines for functional circuit-mapping. *Elife* **8**.

Voltes, A., Hevia, C. F., Engel-Pizcueta, C., Dingare, C., Calzolari, S., Terriente, J., Norden, C., Lecaudey, V. and Pujades, C. (2019). Yap/Taz-TEAD activity links mechanical cues to progenitor cell behavior during zebrafish hindbrain segmentation. *Development* **146**.

Zhang, Q., Xu, H., Zhao, W., Zheng, J., Sun, L. and Luo, C. (2020). Zygotic Vsx1 Plays a Key Role in Defining V2a Interneuron Sub-Lineage by Directly Repressing tal1 Transcription in Zebrafish. *Int J Mol Sci* **21**, 3600.

FIGURE LEGENDS

Fig. 1: Image analysis pipeline and 3D atlas construction.

Schematic depiction of sample processing. First, *Tg[HuC:Kaede]* embryos at 24 hpf displaying magenta in the early differentiated neurons and green in later differentiated neurons are used for supervised training of the Trainable Weka Segmentation 3D algorithm, in which each user inputs a line on areas with signal and areas considered as background across the stack in order to obtain a classifier (e.g., a set of filters and parameters to be used by the algorithm to isolate the signal). For each specimen, as many binary masks as user-generated classifiers can be made and averaged, to obtain a user average segmentation (3D specimen model); this allows the interuser segmentation variability to be assessed, and limits the human bias introduced by the supervised training. Signal similarity threshold between users can then be selected (here, at least >50% was used). User average of each specimen 3D models of a given condition can then registered together using the Fijiyama registration plugin. Once all specimens are properly aligned, the global volume of the signal and the signal distribution are quantified. User averages of each specimen 3D model are then averaged to obtain the final 3D model of a given condition. The resulting 3D model displays a gradient of intensity corresponding to the similarity of signal among users and among specimens, reflective of the overall quality of the signal represented. Thresholding of the specimen 3D models prior to averaging can be used to appreciate the interspecimen variability of the model. Finally, 3D-models can then be overlayed to generate a 3D-atlas.

Fig. 2: The neuronal differentiation domain grows at the expense of the progenitor domain.

(A) Volume quantification of the progenitor domains (PD) and neuronal differentiation domains (NDD) at 24, 36, 48 and 72 hpf. The HuC signal (magenta) corresponds to the NDD, and of the CAAX signal (green) after subtraction of the HuC signal corresponds to the PD. Quantified volumes are presented as mean and SD of *n*=5 samples per time point. Note the increase of the NDD at the expense of the PD. (B–E') Kaede^{Green} in the neuronal differentiation domain of *Tg[CAAX:EGFP;HuC:Kaede]* embryos was photoconverted to Kaede^{Red} at the different indicated times, and embryos were immediately imaged.

Transverse views at the level of rhombomere 3 (r3) and 5 (r5), as indicated. Note that the differentiation territory (magenta) grows over time, while the PD (green) decreases. (F) Table representing the ratio of the volumes of differentiated neurons over total hindbrain (NDD/HB) resulting from the quantification of images shown in B–E (*n*=5). (G) Graph displaying the mean ratios of the NDD over HB, and of PD over HB.

Fig. 3: Differentiated neurons spatially organize according to their birthdate.

(A, C) Raw images of *Tg[HuC:Kaede]* zebrafish embryos at 48 hpf displaying Kaede^{Red} in all neurons born before photoconversion time (24 hpf or 36 hpf) (A), or of Kaede^{Green} in neurons born after each given time (B). Photoconversion allowed us to see the order of neuronal differentiation. (B, D) 3D model transverse views or (B', D') dorsal average projections color-coded according to the neuronal birthdate (early-born neurons in black vs. late-born neurons in white). (E) Volumes of late-born and early-born neurons were quantified (Table 1) and the ratio of early born over total NDD was plotted. Welch *t*-test was performed (****P<0.0001). (F, H, J) Raw data of the hindbrain of *Tg[HuC:Kaede]* zebrafish embryos acquired at 72 hpf upon Kaede^{Green} photoconversion at 24 (F), 36 (H) or 48 hpf (J). (G, I, K) 3D-model transverse views or (G', I', K') dorsal average projections, color-coded according to the birthdate (early-born neurons in black vs. late-born neurons in white). (L) Ratios of Ratios of early-born over total NDD (based on Table 2). One-way ANOVA test was performed with *n*=5 samples per condition. ***P<0.001, ****P<0.0001). All transverse views correspond to r5 level. (M) Distribution of the signal ratio across the antero-posterior (AP), medio-lateral (ML) and dorso-ventral (DV) axes of 3D models displayed in (G', I', K') and plotted as mean (segmented) and non-linear regression (solid).

Fig. 4: Temporal registration of the hindbrain neuronal differentiation domain revealed the relative position of neurons differentiated at distinct time.

(A-A'') 3D-models of *Tg[HuC:Kaede]* embryos acquired at 48 hpf, in which Kaede^{Green} was photoconverted at 24 and 36 hpf, registered and overlaid. Neurons produced before 24 hpf are depicted in black, those produced between 24 hpf and 36 hpf are in magenta, and the

white regions display neurons produced between 36 hpf and 48 hpf. (B-D'') 3D models of *Tg[HuC:Kaede]* embryos acquired at 72 hpf, in which Kaede^{Green} was photoconverted at 24 and 36 hpf (B-B''), at 24 and 48 hpf (C-C'') or at 36 and 48 hpf (D-D''), registered and overlayed on each other. Neurons produced before the earliest of the two photoconversions are depicted in black, those produced in between the two times of photoconversion are in magenta, and the neurons produced from the last time of photoconversion and the time of acquisition in white. (A-D, A'-D') Transverse views at the level of r3 and r5, as indicated. (A''-D'') Sagittal view.

Fig. 5. The temporal registration 3D-atlas can be used as a proxy to reveal the birthdate of gad1b neurons.

(A-C, A'-C') 3D models of gad1b neurons were overlayed with temporal 3D models of differentiated cells at 24 (A-A'), 36 (B-B') or 48 hpf (C-C'). Gad1b neurons produced before the given times (A, 24 hpf; B, 36 hpf; C, 48 hpf) are depicted in magenta, the region of gad1b neurons produced after these given times are colored in white, and non-gad1b neurons produced before (or after) photoconversion are depicted in black or green, respectively. (D) Transverse view of *Tg[HuC:GFP;gad1b:DsRed]* zebrafish hindbrains acquired at 72 hpf. (E) *gad1b* in situ hybridization of 24 hpf embryo. Sagittal view of a maximum intensity projection with anterior to the left. The otic vesicle (ov) contour is depicted.

Supplementary Material 1: FIJI Macros

Table 1

	24hpf	36hpf
late-born neurons N=5, E+06µm³	9.58 ± 1.24	3.86 ± 0.53
early-born neurons N=5, E+06µm³	2.67 ± 1.05	9.53 ± 0.72
early-born neurons / total differentiated neurons	0.22 ± 0,08	0.71 ± 0.02

Table 2

	24hpf	36hpf	48hpf
late-born neurons N=5, E+06µm³	12.81 ± 2.15	7.08 ± 1.42	3.19 ± 0.43
early-born neurons N=5, E+06µm³	3.63 ± 1,30	7.80 ± 1.74	11.65 ± 1.42
early-born neurons / total differentiated neurons	0.22 ± 0.08	0.52 ± 0.11	0.78 ± 0.04

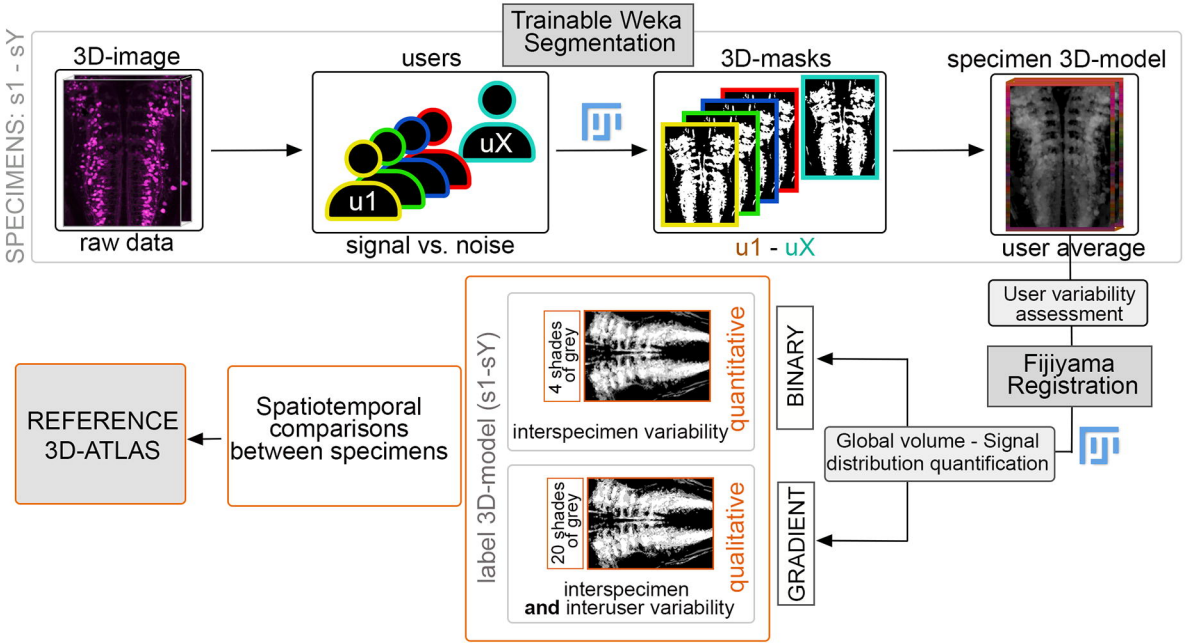
SPECIMENS: s1 - sY
3D-image
raw data
users
u1
uX
signal vs. noise
Trainable Weka Segmentation
3D-masks
u1 - uX
specimen 3D-model
user average
User variability assessment
Fijiyama Registration
Global volume - Signal distribution quantification
BINARY
GRADIENT
label 3D-model (s1-sY)
4 shades of grey
interspecimen variability
quantitative
20 shades of grey
interspecimen and interuser variability
qualitative
Spatiotemporal comparisons between specimens
REFERENCE 3D-ATLAS

A

	24hpf	36hpf	48hpf	72hpf
Progenitor Domain (PD) N=5, E+06µm³	4,72 ± 0,21	3,45 ± 0,43	1,96 ± 0,52	0,99 ± 0,32
Neuronal Differentiation Domain (NDD) N=5, E+06µm³	1,67 ± 0,26	6,77 ± 1,08	10,36 ± 0,72	14,48 ± 0,69
Total Hindbrain (HB) N=5, E+06µm³	6,39 ± 0,46	10,22 ± 0,91	12,32 ± 0,67	15,46 ± 0,82

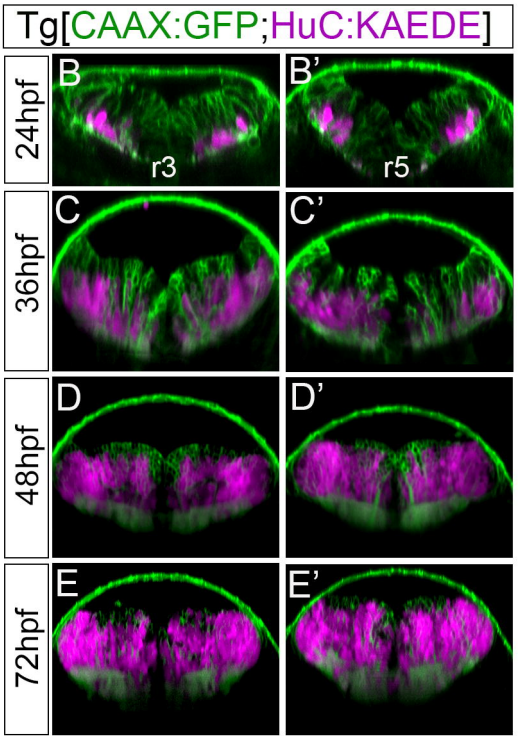

F

	NDD / HB N=5, E+06µm³
24hpf	0,26 ± 0,02
36hpf	0,66 ± 0,06
48hpf	0.84 ± 0.04
72hpf	0.94 ± 0.02

G

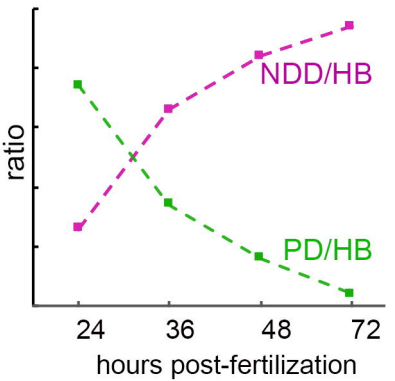

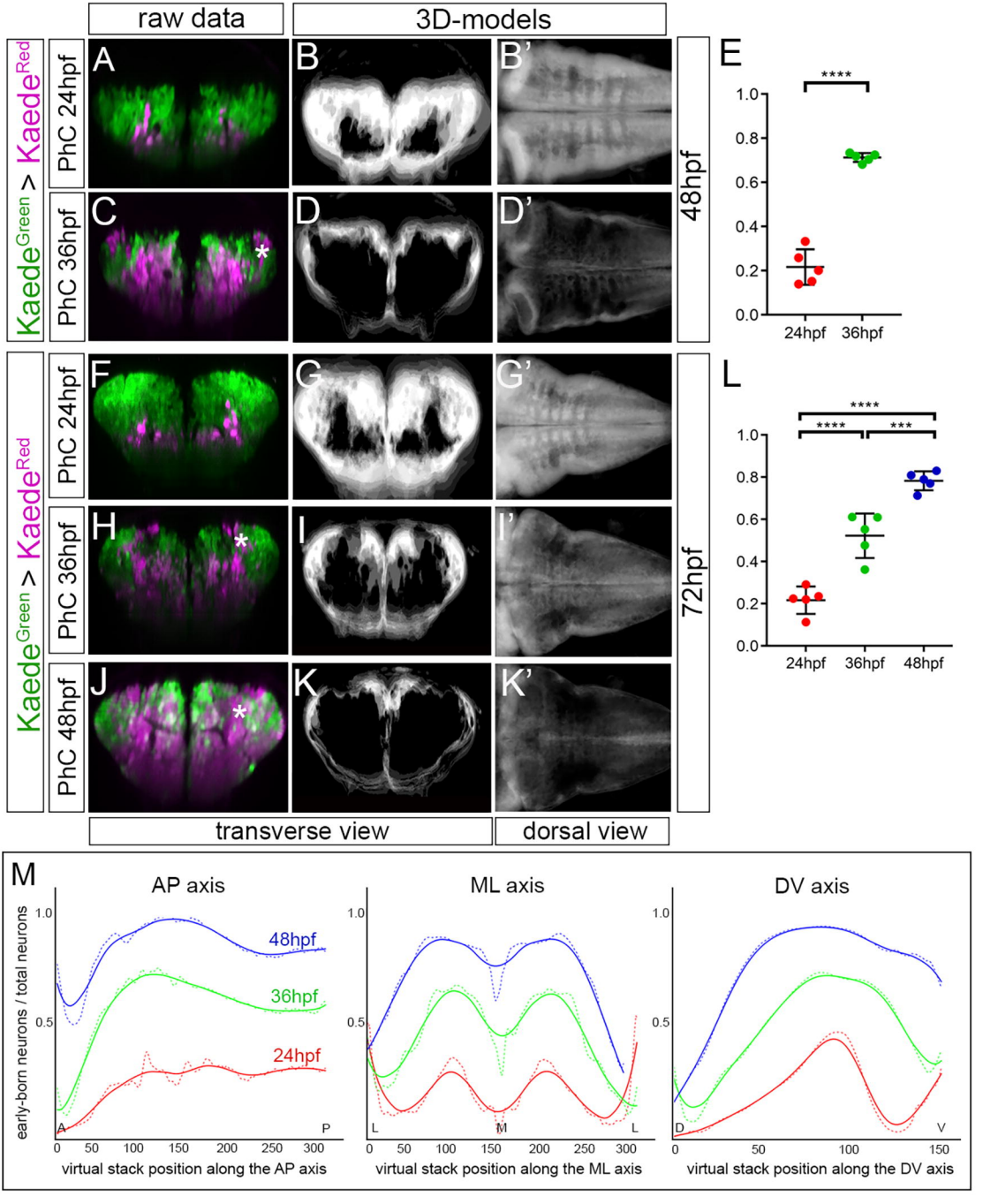
raw data
3D-models
Kaede^Green > Kaede^Red
PhC 24hpf
PhC 36hpf
48hpf
A
B
B'
C
D
D'
E
****
1.0
0.8
0.6
0.4
0.2
0.0
24hpf
36hpf
Kaede^Green > Kaede^Red
PhC 24hpf
PhC 36hpf
PhC 48hpf
72hpf
F
G
G'
H
I
I'
J
K
K'
L
****
****
***
24hpf
36hpf
48hpf
transverse view
dorsal view
M
AP axis
ML axis
DV axis
early-born neurons / total neurons
48hpf
36hpf
24hpf
A
P
L
M
L
D
V
virtual stack position along the AP axis
virtual stack position along the ML axis
virtual stack position along the DV axis

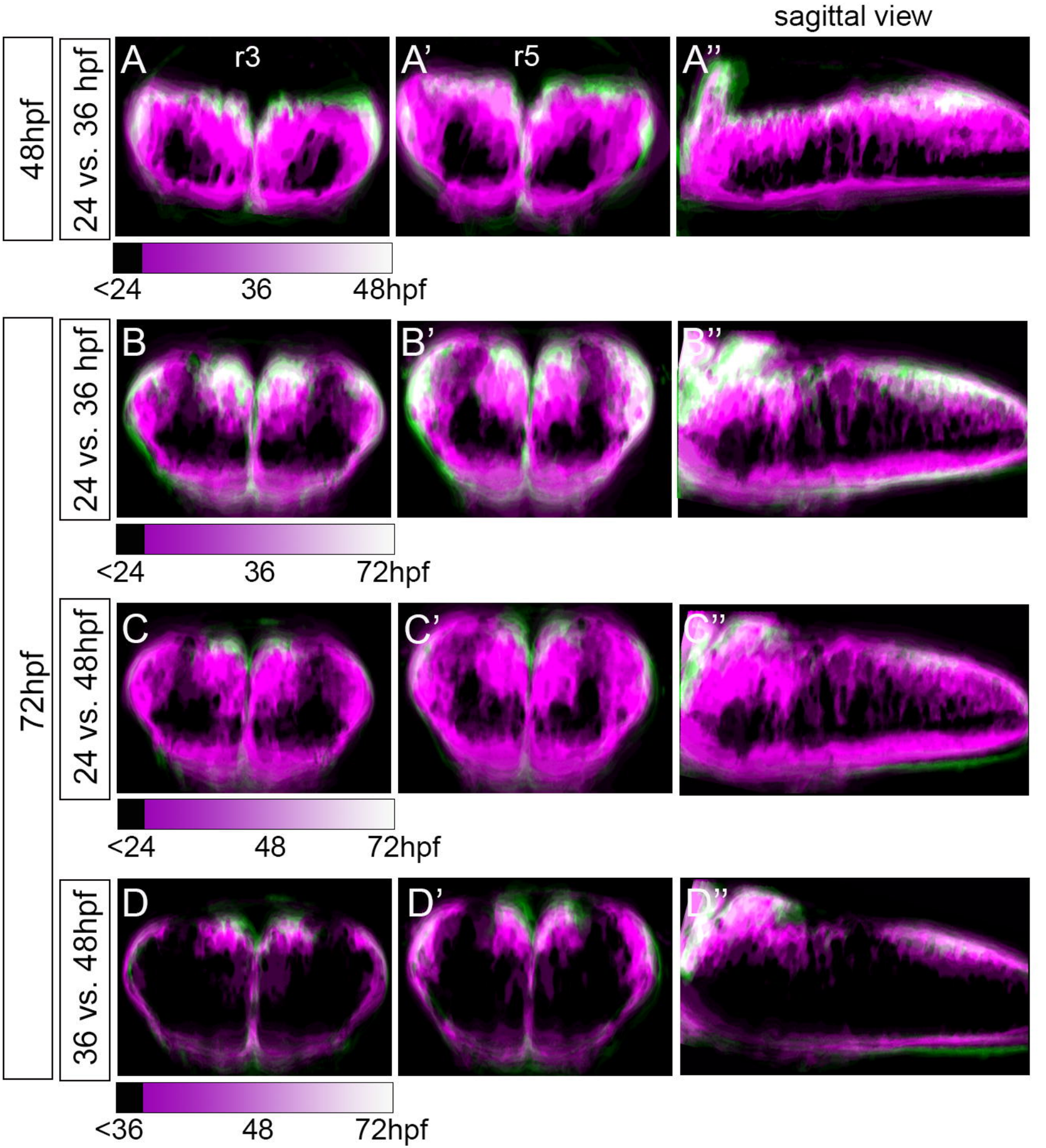
sagittal view
48hpf
24 vs. 36 hpf
A
r3
A'
r5
A''
<24
36
48hpf
72hpf
24 vs. 36 hpf
B
B'
B''
<24
36
72hpf
24 vs. 48hpf
C
C'
C''
<24
48
72hpf
36 vs. 48hpf
D
D'
D''
<36
48
72hpf

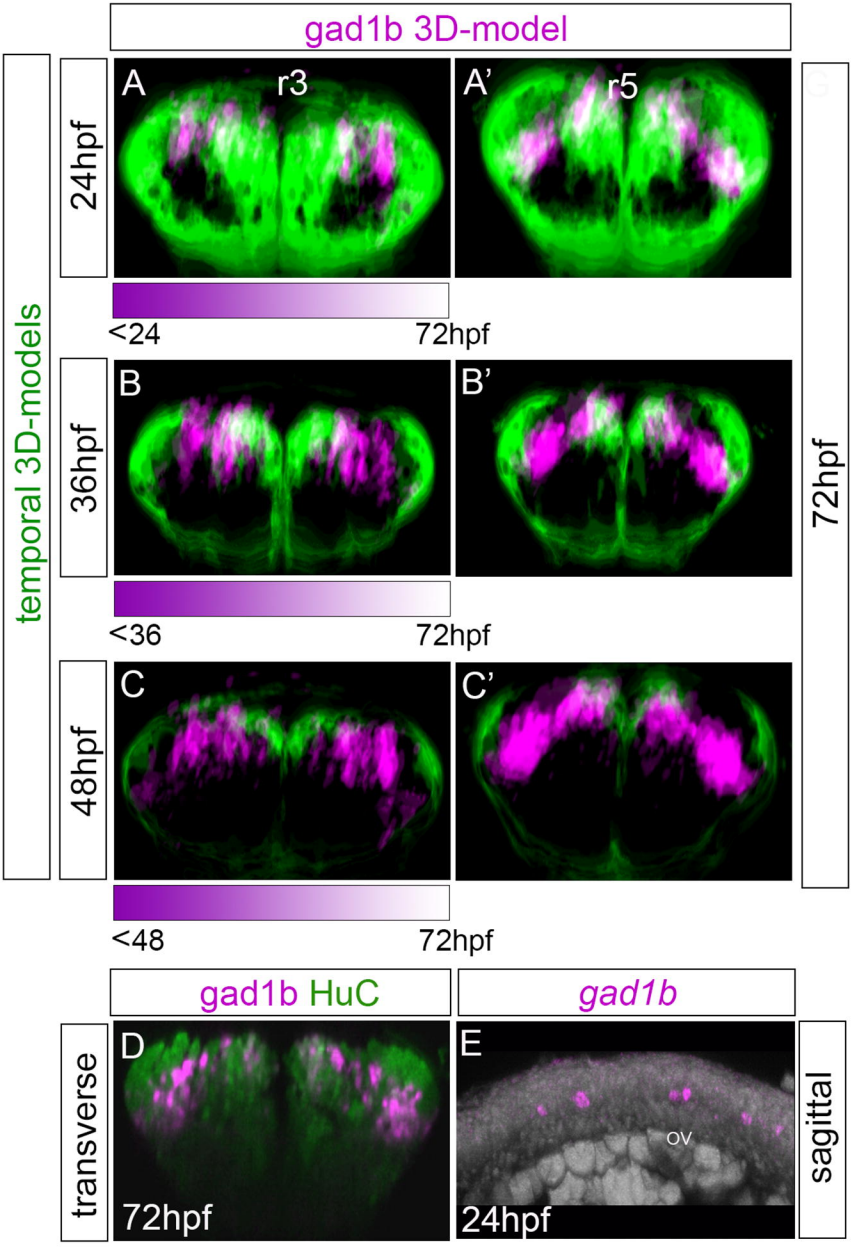
gad1b 3D-model
temporal 3D-models
24hpf
36hpf
48hpf
A
r3
A'
r5
B
B'
C
C'
<24
72hpf
<36
72hpf
<48
72hpf
72hpf
gad1b HuC
gad1b
transverse
sagittal
D
E
ov
72hpf
24hpf